Journal of Molecular Catalysis A: Chemical 308 (2009) 127–133

Contents lists available at ScienceDirect

Journal of Molecular Catalysis A: Chemical

journal homepage: www.elsevier.com/locate/molcata

A one-step route to SAPO-46 using H_3PO_3-containing gel and its application as the catalyst for methanol dehydration

Wenbo Kong, Weili Dai, Niu Li*, Naijia Guan, Shouhe Xiang

Institute of New Catalytic Material Science, College of Chemistry, Nankai University, Tianjin 300071, PR China

ARTICLE INFO

Article history:
Received 2 December 2008
Received in revised form 25 March 2009
Accepted 26 March 2009
Available online 5 April 2009

Keywords:
Silicoaluminophosphates (SAPOs)
Molecular sieve
Catalyst
Methanol

ABSTRACT

SAPO-46 molecular sieve has been synthesized on a new one-step route by using phosphorous acid (H_3PO_3) or the mixture of H_3PO_3 and phosphoric acid (H_3PO_4) as the phosphorus source. It has been found that the pure phase of SAPO-46 could be obtained more conveniently from the H_3PO_3-containing gels at 200 °C. Meanwhile, SAPO-46 with higher crystallinity can be synthesized in a wide range of gel compositions, containing higher silica in the product. As the catalyst for the dehydration of methanol to dimethyl ether (DME), it has exhibited high selectivity for the formation of DME as well as the activity of methanol conversion. Raman and IR have been employed to characterize the initial gel and as-synthesized sample to investigate the formation of SAPO-46 and the one-template-multiple-structures phenomena in the new one-step route, where SAPO-41 or SAPO-46 can be formed according to silica concentration. The transformation of P(III) species in the initial gels to P(V) species during crystallization have been found. It may be the key role for the formation of SAPO-46 on the new route. Besides, the correlation between silica content and the structure type of crystalline products with di-n-propylamine as the template has also been obtained.

1. Introduction

Silicoaluminophosphates (SAPOs) molecular sieves have generated considerable interest as solid acid catalysts since their first synthesis in 1984 [1]. These structures, in general less acidic than aluminosilicates and have been found practical applications as catalysts in industrial processes, such as the selective isomerization of hydrocarbon chains and the conversion of methanol to light olefins (MTO process) [2–7]. In recent years, dimethyl ether (DME), which is now used as a raw material for making chemicals and aerosol propellant such as hair spray, shaving cream to replace ozone-destroying chlorofluorocarbons (CFC), has received attentions as an LPG alternative, transportation fuel in substitution to diesel and power generation [2–5].

Among the various SAPOs, AFS-structure type molecular sieves, which has a unique three-dimensional structure with large-pore, present potential applications. This type molecular sieve is first synthesized in the form of MeAPO and MeASPO by Flanigen and co-workers [8–10]. The structure is based on capped six-membered rings with a unidimensional 12-ring channel system with a free aperture between 7 Å and 8 Å cross-linked through 8-ring windows. AFO-structure contains only 10-ring with a pore size of 4.3 Å × 7.0 Å [11]. AFS-structure silicoaluminophosphates (SAPO-46) appears in 1994 [12]. Similar to other SAPO-based molecular sieves, it is generally synthesized by using phosphoric acid as the source of phosphorus, silica sol and reactive alumina as silica and aluminum source, respectively in the presence of di-n-propylamine (DPA) as the structure directing agent [12]. However the pure SAPO-46 is relatively difficult to be synthesized, as it tends to crystallize along with other DPA directing molecular sieves such as SAPO-11 and SAPO-41 [10,13,14]. So the formation of SAPO-46 needs two crystallizing steps. Firstly it has to be crystallized at 150 °C for 96 h, secondly reacted at 180 °C for a further period of 120 h [12]. Recently, the usages of non-conventional phosphorus sources have shown some distinct effects for crystallizing phosphate-based molecular sieves [15–17]. We have reported the synthesis of SAPO-41 and SAPO-47 molecular sieves by using H_3PO_3 as phosphorus source. H_3PO_3-containing gels have exhibited some competitive effects with organic amines on directing the formation of aluminophosphate-based molecular sieves [18,19]. In the present work, by using H_3PO_3 or the mixture of H_3PO_3 and H_3PO_4 as the source of phosphorus (denoted as P source afterwards), the preparation of SAPO-46 in aqueous system is described. Meanwhile, thermal stability of the as-synthesized SAPO-46, which is lower than that of like SAPO-5 [20] and SAPO-37 [21], has been improved by increasing the Si content of the framework. IR and Raman spectroscopes have been used to detect the transformation of P(III) species to P(V) species during the crystallization procedure

* Corresponding author. Tel.: +86 22 23509932; fax: +86 22 23499992.
E-mail address: liniu@nankai.edu.cn (N. Li).

1381-1169/$ – see front matter © 2009 Elsevier B.V. All rights reserved.
doi:10.1016/j.molcata.2009.03.036

and the slight interaction of the template-framework in SAPO-46. Additionally, the catalytic properties of SAPO-46 on the transformation of methanol to dimethyl ether (DME) have been studied. It has showed high selectivity to DME in collective products with less coke formation tendency.

2. Experimental

2.1. Reactants

Phosphorous acid (>99%) and di-n-propylamine (>95%) were purchased from Tianjin Yaohua Chemical and Acros Organics. Pseudoboehmite (water loss at 600 °C being 34.75 wt.%) was purchased from Shandong Aluminum Plant. Phosphoric acid (>99%) was purchased from Tianjin Chemical. Silica sol (5.9 M SiO_2) was purchased from Qindao Chemical.

2.2. Synthesis of SAPO-46

2.2.1. Using H_3PO_3 as the phosphorus source

Typically, 1.8 g of solid H_3PO_3 was dissolved in 20 ml deionized water, and then H_3PO_3 solution was added slowly to 1.7 g of pseudoboehmite. The mixture was stirred for about half an hour until it became homogeneous. Subsequently, 4.6 ml of di-n-propylamine (denoted as DPA afterwards) were added into it dropwise under vigorous stirring. Then, 1.1 ml aqueous silica sol was added. The reaction mixture had the following molar composition: $1.0Al_2O_3{:}2.0H_3PO_3{:}4.0DPA{:}100H_2O{:}\ 0.6SiO_2$ with gel pH = 8. The mixture was sealed in a Teflon-lined stainless-steel autoclave and heated at 200 °C under autogeneous pressure.

2.2.2. Using H_3PO_3 and H_3PO_4 as the mixed phosphorus source

Typically, 0.91 g of H_3PO_3 was dissolved in 10 ml of deionized water, then 1.1 ml H_3PO_4 was added slowly to H_3PO_3 solution. The mixture was added to 2.1 g of pseudoboehmite and then 10 ml of deionized water was added in. After stirred for about half an hour, then 6.1 ml DPA was added in dropwise under vigorous stirring. Subsequently, 1.1 ml aqueous silica sol was added. The typical molar composition of the reaction mixture is $1.2Al_2O_3{:}1.0H_3PO_3{:}1.5H_3PO_4{:}4.0DPA{:}100H_2O{:}0.6SiO_2$. The mixture was sealed in a Teflon-lined stainless-steel autoclave and heated at 200 °C under autogenous pressure (Table 1).

2.3. Characterization

X-ray powder diffraction (XRD) patterns of the as-synthesized products were recorded on a Rigaku D/MAX-2500 diffractometer with Ni-filtered Cu Kα radiation (λ = 1.5418 Å). The IR spectra were recorded by Brucker Vector 22 FT-IR spectrometer. Raman spectrometer used was Renishaw in via spectroscopy system. The laser used was argon ion laser with 514.5 nm excitation source with power output of 20 mW. Element analysis was performed on an Elementar Varioel element analyzer. Thermal analysis was performed on Netzsch STA 409 PC thermal analyzer at a heating rate of 10 °C/min in nitrogen. The crystal morphology and electron probe microanalysis and chemical compositions of the products were performed with a Hitachi X-650 scanning microscope.

2.4. Catalytic reaction

Before the test, the SAPO-46 was calcined in air at 550 °C for 2 h to remove the organic template completely. The dehydration of methanol to DME was carried out on a fixed-bed stainless-steel reactor and detected with an on-line GC. The experiments were performed on atmospheric pressure at 350 °C, 450 °C and 585 °C, respectively. For each case, 0.6 g of HSAPO-46 catalyst (grain size 20–40 mesh) was used. Nitrogen saturated by pure methanol (11% MeOH in N_2) was used as feed with the gas mass space velocity (WHSV) 1.0 h^{-1}. It was 30 min for saturating the N_2 stream with methanol.

3. Results and discussion

3.1. Synthesis and initial characterization

In conventional synthesis procedure using H_3PO_4 as phosphorus source, SAPO-46 can only be obtained from a two-step route. It needs first to be crystallized at 150 °C for an initial period of 96 h, and then another period of 120 h at 180 °C would be expended [12]. However, in the present studies by using H_3PO_3 as the source of phosphorus, the pure SAPO-46 can be crystallized directly at 200 °C for only 72 h in the system of $Al_2O_3/SiO_2/H_3PO_3/DPA/H_2O$ or $Al_2O_3/SiO_2/H_3PO_3/H_3PO_4/DPA/H_2O$. X-ray powder diffraction patterns of as-synthesized samples are shown in Fig. 1. It closely resembles to that of SAPO-46 phase reported in the literature [12]. SEM photographs confirm the phase purity prepared in this synthesis route (Fig. 2). Apart from this, the range of silica concentration for crystallizing pure SAPO-46 phase has been extended from $0.3 < SiO_2/Al_2O_3 < 0.6$ [13] to $0.3 \leq SiO_2/Al_2O_3 \leq 1.25$. Samples in Fig. 1 have shown the result for synthesizing SAPO-46 in gels with different silica concentration (the molar ratio of SiO_2/Al_2O_3 are 0.4, 0.8, 1.0, 1.3, respectively). Especially in the gels with $SiO_2/Al_2O_3 = 0.8$, the product shows the best crystallinity (Fig. 1B). A lower silica concentration, for example, in the range of $0.2 < SiO_2/Al_2O_3 < 0.3$, it led to the mixtures of SAPO-41 and SAPO-46 (Table 1 E). $SiO_2/Al_2O_3 \leq 0.2$ is the identical synthesis conditions to prepare pure SAPO-41 phase (Table 1 F). On the opposite, if $SiO_2/Al_2O_3 > 1.5$, no crystallization product can be obtained even if the duration was prolonged from 3 to 7 days.

Other factors, such as amounts of H_2O, DPA have also shown their impact on the formation of SAPO-46. It can also be seen from Table 1 and Fig. 3 that when $H_2O/Al_2O_3 < 150$, pure SAPO-46 is obtained (Fig. 3A). A higher H_2O content ($150 \leq H_2O/Al_2O_3 < 200$)

Table 1
Gel compositions and crystallization conditions of SAPO-46.

Sample	Reactant composition						Crystallization condition		Product
	Al_2O_3	H_3PO_3	H_3PO_4	SiO_2	DPA	H_2O	Temp (°C)	Time (day)	
I	1.0	2.0	0	0.6	3.0	100	200	6	Pure SAPO-46
A	1.2	1.0	1.5	0.6	4.0	100	200	3	Pure SAPO-46
B	1.2	0.5	1.5	1.5	4.0	100	200	3	Pure SAPO-46
C	1.2	1.0	1.5	0.4	4.0	100	200	3	Pure SAPO-46
D	1.2	1.5	1.5	0.6	4.0	100	200	3	Pure SAPO-46
E	1.2	0	2.0	0.6	4.0	100	200	3	SAPO-11, SAPO-46
F	1.2	1.0	1.5	0.2	4.0	100	200	3	Pure SAPO-41
G	1.2	1.0	1.5	0.6	2.0	100	200	3	Pure SAPO-11
H	1.2	1.0	1.5	0.6	2.0	180	200	3	SAPO-43, SAPO-46

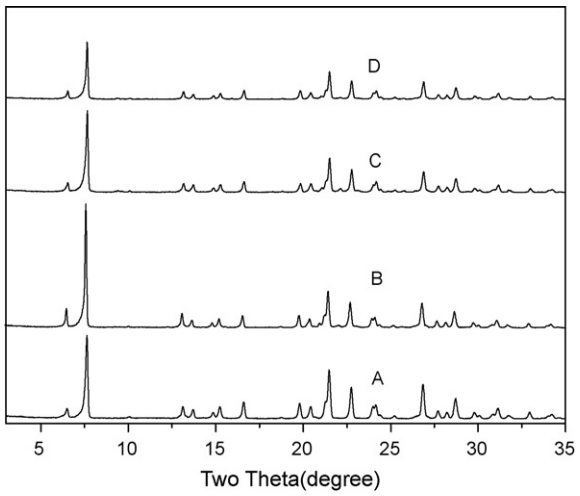

Fig. 1. XRD patterns of SAPO-46 with different Si content. The molar ratios of SiO_2/Al_2O_3 are (A) 0.4; (B) 0.8; (C) 1.0; (D) 1.3.

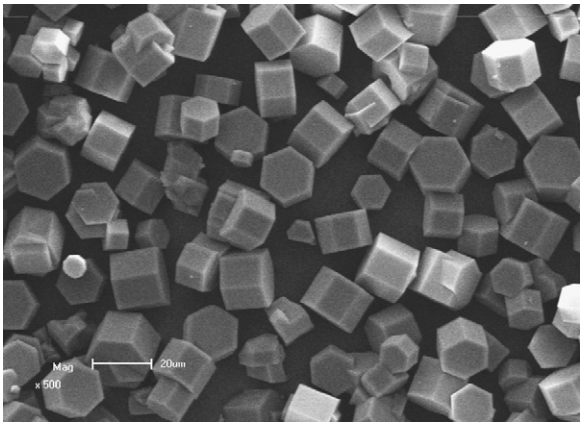

Fig. 2. SEM images of SAPO-46.

will lead to a mixed product of SAPO-46 and SAPO-43 (Fig. 3B). If the ratio (H_2O/Al_2O_3) is above >200, SAPO-11 is present as the impurity (Fig. 3C). As for the DPA, when $DPA/Al_2O_3 \geq 3$, pure SAPO-46 can be synthesized, whereas in the range of $2 < DPA/Al_2O_3 < 3$, SAPO-11

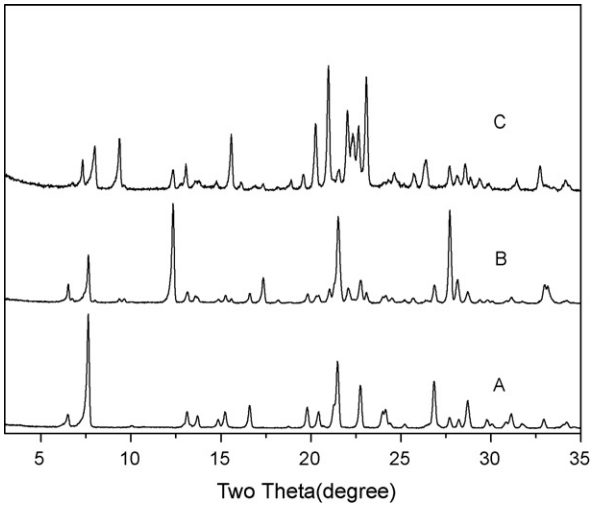

Fig. 3. XRD patterns of crystallization products with H_2O/Al_2O_3 at A: 50; B: 150; C: 200.

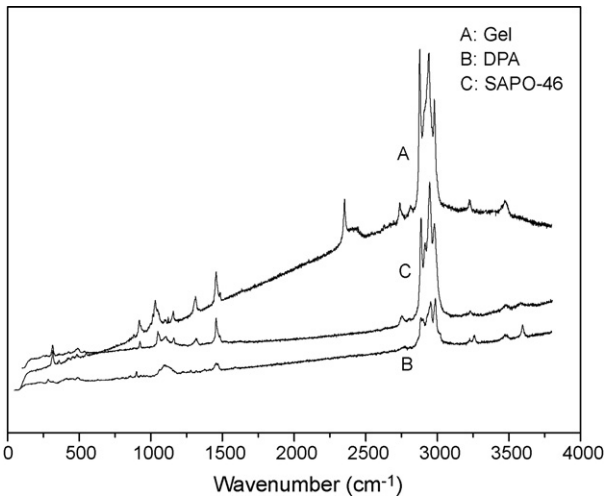

Fig. 4. Raman spectra of (A) silicoaluminophosphite gel, (B) DPA and (C) as-synthesized SAPO-46.

appears as the impurity. When DPA/Al_2O_3 ratio is low than 3, pure SAPO-11 can be obtained [13].

3.2. Raman and IR investigation of the initial gel and as-synthesized sample to identify the key role in the new one-step route

In the case using H_3PO_4 as phosphorus source, two-step route has to be employed to obtain pure SAPO-46 phase, which is first crystallized at 150 °C for 96 h, and then another 120 h at 180 °C [12]. How can it to be obtained as a pure phase directly at 200 °C for only 72 h? It is the presence of H_3PO_3 and the silicoaluminophosphite gel formed from it. In order to study the important role of them, a silicoaluminophosphite gel with its original composition $1.0Al_2O_3:P_2O_3:3.0DPA:0.6SiO_2:100H_2O$ (Table 1, sample I) was dried at room temperature. The Raman and IR spectra of the gel and its crystallization product SAPO-46 are obtained and shown in Figs. 4 and 5. The assignments of the bands of SAPO-46 (Table 2) have been based on the published works of other researchers [22–26]. The intense Raman band (Fig. 4) and the most intense, wide and complex band in IR spectra (Fig. 7) are in the 1000–1300 cm^{-1} region, which corresponds to P–O vibration modes [23,24]. And the intensity and position of the P–O vibration bands of silicoaluminophosphite gel differ significantly from that of SAPO-46. For example, in IR spectra, the most intense band of silicoaluminophos-

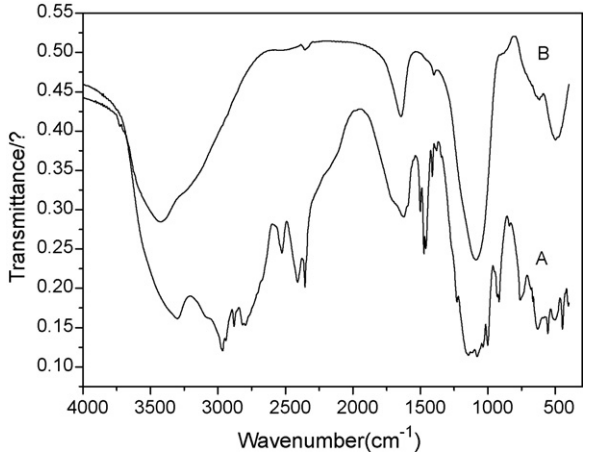

Fig. 5. IR spectra of (A) silicoaluminophosphite gel and (B) as-synthesized SAPO-46.

Table 2
Assignment of vibration bands of SAPO-46 [22–26].

Wavenumber (cm^{-1})		Assignment
IR	Raman	
3300	3200–3300	N–H vibration mode
2750–3000	2750–3000	C–H stretching vibration
2353, 2413	2353, 2439	P–H vibration
1622		O–H vibration of H_2O
1380–1500	1400–1500	Deformation vibration of CH_3 and CH_2
1000–1300	1030–1300	P–O stretching vibration
~920	~920	P–O stretching vibration of HPO_2^{-3}
650–750	600–750	Bending vibration of Al–O
400–600	90–530	Oxygen atom vibration in T–O–T (T–O–T bending vibration)

phite gel is at 1087 cm^{-1}, but in that of SAPO-46, the most intense band is at 1118 cm^{-1}. Meanwhile, the band at 916 cm^{-1} in the spectra of the gel, which attributes to P–O vibration of HPO_3^{2-}, disappears upon crystallization. These differences probably result from the different oxidation state and the different chemical environment of P element. It is noticeable that, the band in the region of 2300–2500 cm^{-1} in Raman and IR spectra of silicoaluminophosphite gel, which belongs to P–H vibration, disappears in that of SAPO-46. This means that, during the crystallization from silicoaluminophosphite gel to SAPO-46, P(III) species transforms into P(V) species. The transformation between the solid state species (aluminophosphites to aluminophosphates) has been detected before on the synthesis of $AlPO_4$-5 and SAPO-47 using H_3PO_3 as the phosphorus source [27]. It means that pseudo-tetrahedral HPO_3 may co-exist with tetrahedral PO_4 in the intermediates. This reaction probably results in the highly strained tetrahedral T-atom sites present in the framework and acts as the key role on the formation of SAPO-46. It is just like the slow and in situ releasing of the amine in the reaction batch being a key factor for the formation of the AFO type material [28].

3.3. The correlation between silica content and the structure type of crystalline products with di-n-propylamine as the template

In the domain of SAPO materials, di-n-propylamine has been used to direct the synthesis of at least eight different $AlPO_4$-based structure types, such as SAPO-11, SAPO-31, SAPO-39, SAPO-41, and SAPO-46 [29], which was called as one-template-multiple-structures phenomena [30,31]. The changes of DPA concentration in the reacting mixture is the key to the formation these compounds (SAPO-11, SAPO-31, SAPO-41) [32]. However, in the synthesis of SAPO-46 and SAPO-41, silica content plays an important role. It has been found from Table 1 that the templating effects of DPA are not as critical for the formation of AFS (SAPO-46) or AFO (SPO-41) as for other frameworks (SAPO-11 with AEL code, SAPO-31 with ATO code). Both SAPO-41 and SAPO-46 can be prepared at a typical molar composition with the same DPA concentration ($DPA/Al_2O_3 = 4.0$). It is noted that a higher silica concentration ($SiO_2/Al_2O_3 \geq 0.3$) yields SAPO-46, silica concentration in the range of $0.2 < SiO_2/Al_2O_3 < 0.3$ crystallizes the mixture of SAPO-41 and SAPO-46, whereas at lower silica concentration ($SiO_2/Al_2O_3 \leq 0.2$), it results in the formation of pure SAPO-41, whether in the one-step or in two-step synthesis route [12]. What cause these results?

Investigations by Lewis et al. concerning the number and conformation of organic amines present in the cage of chabazite structure enlighten us to attribute these results to the host–guest interactions between framework and organic amines [33]. Their studies have shown that two distinct aluminophosphate structures, $AlPO_4$-5 (AFI code) and the chabazitic $AlPO_4$-34 polymorph (CHA), may be synthesized as Co-AlPOs from the same gel, depending on the concentration of Co^{2+} and template [34]. The competitive formation of the AFI and CHA structures from a CoAlPO gel is controlled by the uptake of template and of Co(II) ions from the gel. Their studies identify that CHA structure is thermodynamically less stable than the AFI structure, higher (cationic) concentrations of template favor the formation of it, induced by higher (negatively charged) Co^{2+} substitution levels in the framework, the binding of the template to the CHA framework is significantly higher than in the AFI structure [34,35]. Whereas the more stable AFI structure is accessible at low template concentration with lower Co^{2+} substitution levels. In the gel lack of Co, $AlPO_4$-5 (AFI structure code) is formed rapidly, whereas CHA phase does not appear even at a lower Co concentration. On the contrast, it has often been obtained from higher Co concentration systems [33], as well as higher Mg and Si concentration favor formation of MgAPO-34 and SAPO-44 over MgAPO-5 and SAPO-5, respectively [36]. The formation of the CHA phase appears to be strongly correlated to the presence of Co or other substituted elements, since simply increasing the template concentration does not induce its formation. It means that for the competitive formation of several frameworks in a crystallizing mixture, the more stable structures being accessible at low template concentration with low heteroatom to compensate the template charge. On the contrast, to form a thermodynamically less stable phase, it is necessary to increase the relative template concentration and in turn, requires sufficient heteroatom present in the framework. Maybe structures of SAPO-46 and SAPO-41 caused by Si content also attributed to the concentration of DPA?

Fig. 6 shows the TG and DSC results of the as-synthesized SAPO-46. Weight loss takes place in three steps. Water molecules are lost first (2.8%) followed by the loss of the template molecules in two steps. DSC curve shows an endothermic and two exothermic peaks corresponding to these processes. The two steps removal of the template could be due to the different adsorption ability produced by different acid strength in the framework. The main weight loss of SAPO-46 is about 18.0%, which corresponds to the removing of DPA (from 230 °C to 700 °C). This means that approximately 7.7 Pr_2NH molecules are present in one unit cell, which is in good accordance with the result of element analysis (with C 12.5 wt%, H 3.5 wt%, N 2.62 wt%, and 8 Pr_2NH present per unit cell). As for SAPO-41 (Fig. 7), it is found that the main weight loss related to DPA is only 8.0% (from 150 °C to 700 °C), about 1.2 Pr_2NH molecules per unit cell are present in SAPO-41 [13,37,38]. Taking into the different T atoms per unit cell, there are 0.143 DPA in SAPO-46 and 0.06 DPA in SAPO-41 corresponding per T atom. Evidently, DPA molecules in SAPO-46 channels are more than SAPO-41, even though there is the same concentration DPA in the initial gels (Table 1 A and F).

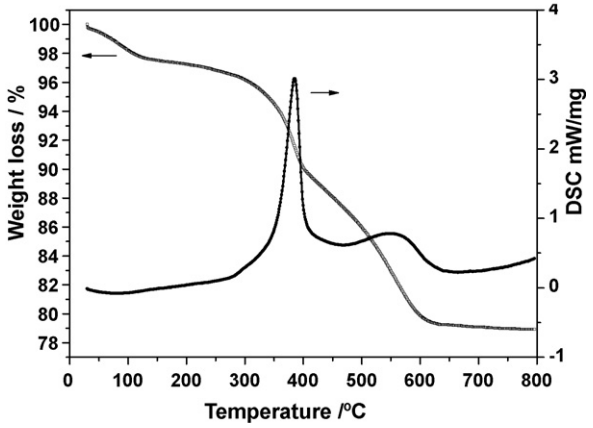

Fig. 6. TGA and DSC curves of as-synthesized SAPO-46.

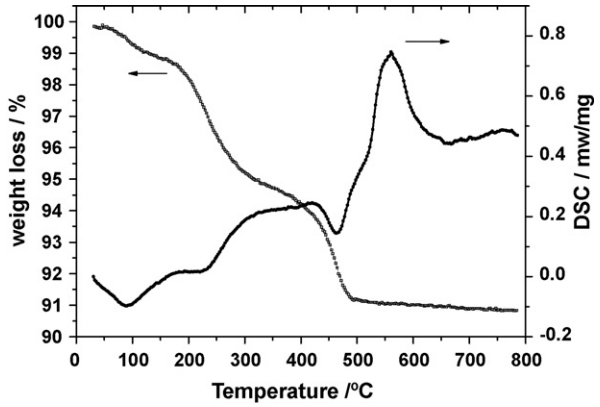

Fig. 7. TGA and DSC curves of as-synthesized SAPO-41.

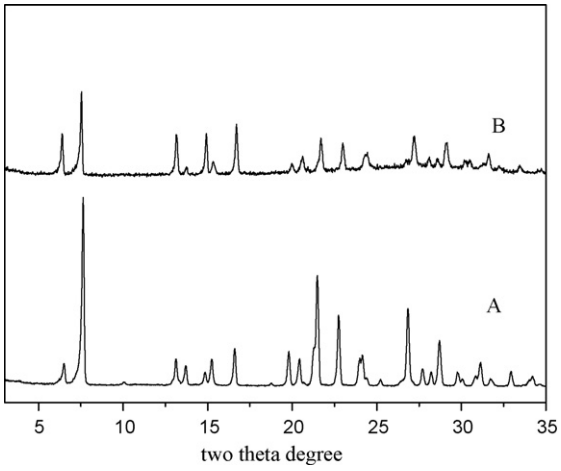

Fig. 8. XRD patterns of SAPO-46 from SiO_2/Al_2O_3 = 0.5 gel (A) as-synthesized sample; (B) calcined at 550 °C for 2 h.

So we can infer that the structure of SAPO-46 is less stable than SAPO-41, its framework is only formed at higher template concentration level and in turn, requires higher Si heteroatom present in the framework.

Prakash et al. have once reported that the thermal stability of the as-synthesized SAPO-46 was lower than those of materials like SAPO-5, MgAPO-36 and SAPO-37 [13]. Our investigations have also shown (Fig. 8) that after calcinations, the XRD peak intensities corresponding to SAPO-46 (Table 1 A) decreased more dramatically. On the contrary, the as-synthesized SAPO-41 is thermodynamically stable even for calcined at 800 °C for 2 h (Fig. 9). These results are in agreement with our speculation on the stability of SAPO-46 and SAPO-41, and can be used to evaluate the competing formation in the one-template-multiple-structures phenomena of SAPO molecular sieves. Moreover, it is interesting that the thermal stability of SAPO-46 may be improved when increasing the content of framework silica. As seen in Tables 1 and 3, Si content in sample SAPO-46A (Table 1. A, molar ratio: SiO_2/Al_2O_3 is 0.5 in gel, and Si/Al is 0.34 in framework) is less than SAPO-46B (Table 1. B, molar ratio: SiO_2/Al_2O_3 is 1.25 in gel, and Si/Al is 0.67 in framework) in both gels and crystallization products. When calcining at 550 °C for

Table 3
Chemical analysis of the SAPO-46 (molar composition).

Sample	Si	P	Al
SAPO-46 (A)	0.20	0.42	0.58
SAPO-46 (B)	0.35	0.33	0.52

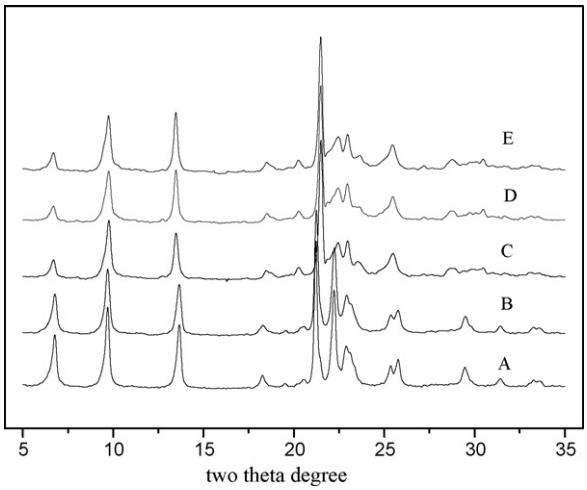

Fig. 9. XRD patterns of SAPO-41 from SiO_2/Al_2O_3 = 0.15 gel (A) as-synthesized sample; (B)–(E) calcined at 550 °C, 600 °C, 700 °C and 800 °C for 2 h, respectively.

2 h, the intensity of the main diffraction peaks in XRD patterns corresponding to SAPO-46A decreases more dramatically, whereas in SAPO-46B, it is only half decrease after calcining, as well as the thermal stability of AFI framework being boost up by incorporating Si composition in the structure [39,40].

Our previous works have reported the Raman investigation in the multiple-templates-one-structure from the vibration information on the host–guest interaction of CHA-type SAPO molecular sieves [41,42]. In the one-templates-multiple-structure process, Raman spectra of host-guest interaction between DPA and SAPO-46 or SAPO-41 frameworks have been shown in Fig. 10. The vibration modes of DPA in the region of 1400–1500 cm^{-1} and 2600–3100 cm^{-1}, which can be assigned to the deformation and to stretching vibration of C–H [22–24], also appear in the spectra of silicoaluminophosphite gel and SAPO-46. As DPA trapped within the pores of $AlPO_4$-based materials always exist as its protonated form [30,42], Fig. 10 has also displayed the Raman spectra of DPA, protonated-DPA (adding dilute hydrochloric acid to the metric DPA) and DPA containing gel. The main spectral features of DPA are the antisymmetric vibrations of CH_2 at 2873 cm^{-1}, 2901 cm^{-1}, 2932 cm^{-1} and 2962 cm^{-1}, respectively, which has been described in Ref. [43]. Both the spectra of protonated DPA and reacting gel are similar to each other with the C–H stretching vibration shifting to 2880 cm^{-1}, 2909 cm^{-1}, 2938 cm^{-1}, and 2966 cm^{-1}, respectively.

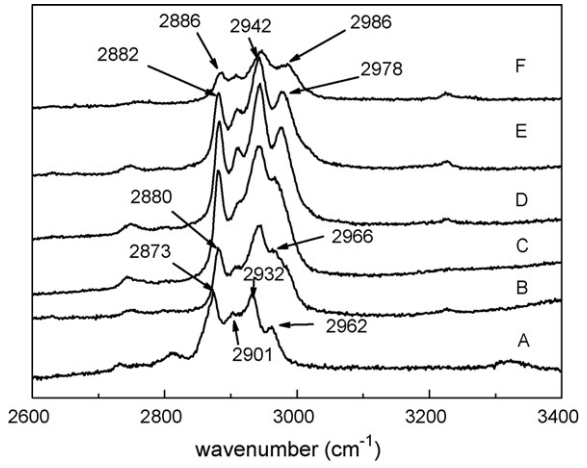

Fig. 10. Raman spectra of (A) DPA; (B) protonated DPA; (C) gel; (D) as-SAPO-46 with lower Si content; (E) as-SAPO-46 with higher Si content; (F) as-SAPO-41.

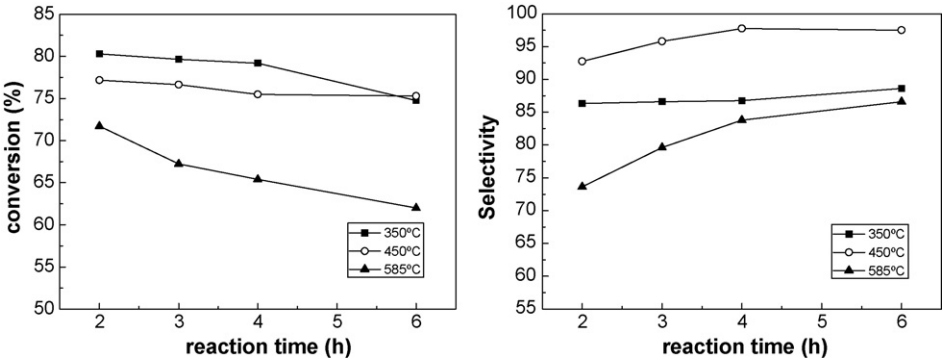

Fig. 11. Methanol conversion (A) and the selectivity (B) of DME at 350 °C, 450 °C, and 585 °C, with nitrogen saturated by pure methanol (11% MeOH in N_2) was used as feed with the gas mass space velocity (WHSV) 1.0 h^{-1}.

As for the case of SAPO-46, the antisymmetric vibrations of CH_2 shift to higher wave number with three main vibrations at 2882, 2942, and 2978, reflecting the interaction of the channel framework and protonated-DPA. Meanwhile it has been found that the bands of SAPO-41 is slightly shifted to higher wave number than that of SAPO-46 with three major bands at 2986 cm^{-1}, 2947 cm^{-1}, and 2986 cm^{-1}. The shift also reflects the difference of SAPO-41 and SAPO-46 on the confined space around the organic molecule [43]. It is obvious that channels in SAPO-46 structure are circled by 12 tetrahedra (12-ring), which differ from the 10-ring channels in SAPO-41. The confined space of DPA in SAPO-41 is smaller than that in SAPO-46. On the other hand, the directing effect of protonated-DPA (reacting with dilute hydrochloric acid) has been tested by adding it to the gel (Al_2O_3:H_3PO_3:H_3PO_4:H_2O). Then the acidic system has been crystallized at 200 °C for 3 days. The tridymite phase has been obtained, which is just like what has been synthesized directly from an $AlPO_4$ gel without any organic template present in the system.

3.4. Catalytic reaction for dehydration of methanol to DME over SAPO-46 catalysts

Fig. 11 displays the catalytic performance of SAPO-46 on methanol dehydration. It shows the results of methanol conversion and selectivity of DME at several reaction temperatures. Reacting at 350 °C for 6 h, the methanol conversion decreased from 80% to 75%. At 450 °C, the methanol conversion almost keeps constant above 75%. For example, at 450 °C for 2 h and 6 h, the methanol conversion is 77.1% and 75.9%, respectively. It means that SAPO-46 has still the activity after reacting for 6 h with the selectivity of DME above 95%. When the reaction was performed at 585 °C, accompanying with the deactivation of catalyst, the methanol conversion has decreased from 72% to 62% for only 2 h. It indicates that the catalytic activity of SAPO-46 decreased clearly with the reaction temperature increasing from 450 °C to 585 °C. The coking formation over catalyst surface is a temperature related reaction. So at the temperature above 450 °C, the deactivation rate of the SAPO-46 is depended on the increasing of coke formation.

The selectivity of DME (Fig. 11B) also keeps constant (about 98%) at 450 °C during the reaction period with the selectivity of DME, CH_4, C_4, C_6 being 98.7%, 0.6%, 0.2% 0.4%, respectively at 2 h and 99.0%, 0.4%, 0.1% 0.4%, respectively at 6 h. Although the selectivity of CH_4 increases gradually when the reacting temperature increases from 450 °C to 585 °C, DME is still the main product on SAPO-46 with the selectivity over 80%. It is well known that on many zeolite catalysts, the DME selectivity of dehydration of methanol is low 68.23% accompanying with the quickly deactivating of catalyst [44]. What cause this? In previous investigations it has been demonstrated that the main reason for catalyst deactivation in the methanol dehydration step is the production of coke over the strong acid sites [45–47]. Owing to the unique three-dimensional structure with large-pore (12-ring) in SAPO-46 and less strong acid sites than zeolite bringing on less tendency to coke formation, the catalyst of SAPO-46 can retain the high selectivity and activity at lower temperature.

4. Conclusions

The present investigation describes a new one-step route to synthesize pure AFS-type SAPO-46. In the presence of phosphorous acid (H_3PO_3), SAPO-46 can be obtained in a wider range of gel compositions more conveniently. Raman and IR investigation indicate that P(III) species have transformed to P(V) species during crystallization. When the mixed phosphorus source of H_3PO_3 and H_3PO_4 are used, the crystallization speed of SAPO-46 is accelerated. Meanwhile Raman spectra reveal that the DPA molecules occluded are present as the protonated form. In addition, SAPO-46 has high catalysis selectivity and activity of dehydration of methanol to dimethyl ether (DEM).

Acknowledgements

This work was supported by the National Natural Science Foundation of China (NSFC. 20873069) and National Basic Research Program of China (2009CB623502).

References

[1] J.A. Rabo, R.J. Pellet, P.K. Coughlin, E.S. Shamshoum, Stud. Surf. Sci. Catal. 46 (1989) 1.
[2] G. Sastre, D.W. Lewis, C.R.A. Catlow, J. Mol. Catal. A 119 (1997) 349.
[3] D. Hasha, L. Saddalrriaga, P.E. Hataway, D.F. Cox, M.E. Davis, J. Am. Chem. Soc. 110 (1988) 2127.
[4] S. Wilson, P. Barger, Micropor. Mesopor. Mater. 29 (1999) 117.
[5] Z. Wang, Y. Jiang, M. Hunger, Catal. Today 113 (2006) 102.
[6] G.H. Geng, F. Zhang, Z.X. Gao, L.F. Zhao, J.L. Zhou, Catal. Today 93 (2004) 485.
[7] J.M. Campelo, F. Lafont, J.M. Marinas, J. Chem. Soc., Faraday Trans. 91 (1995) 4171.
[8] E.M. Flanigen, B.M. Lok, R.L. Patton, S.T. Wilson, Proceedings of 7th International Zeolite Conference, Elsevier, Amsterdam, 1998, p. 103.
[9] S.T. Wilson, E.M. Flanigen, ACS Symp. Ser. 398 (1989) 329.
[10] E.M. Flanigen, Patton, S.T. Wilson, Stud. Surf. Sci. Catal. 37 (1988) 13.
[11] J.M. Bennett, B.K. Marcus, Stud. Surf. Sci. Catal. 37 (1988) 269.
[12] A.M. Prakash, C.V.V. Satyanarayana, S. Ashtekar, D.K. Chakrabarly, J. Chem. Soc. Chem. Commun. (1994) 1527.
[13] A.M. Prakash, S. Ashtekar, K. Dipak, Chkrabarty, J. Chem. Soc., Faraday Trans. 91 (1995) 1045.
[14] A.K. Sinha, C.V.V. Satyanarayana, D. Srinivas, S. Sivasanker, P. Ratnasamy, Micropor. Mesopor. Mater. 35 (2000) 471.
[15] A. Tuel, S. Caldarelli, A. Meden, L.B. McCusker, C. Baerlocher, A. Ristic, N. Rajic, G. Mali, V. Kaucic, J. Phys. Chem. B 104 (2000) 5697.
[16] S. Neeraj, C.N.R. Rao, A.K. Cheetham, J. Mater. Chem. 14 (2004) 814.
[17] D.A. Lesh, R.L. Patton, N.A. Woodward, Eur. Pat. Appl. 293939.
[18] Y. Ma, N. Li, S. Xiang, Micropor. Mesopor. Mater. 86 (2005) 329.

[19] Y. Ma, N. Li, X. Ren, S. Xiang, N. Guan, J. Mol. Catal. A: Chem. 250 (2006) 9.
[20] A.M. Prakash, S. Unnikrishnan, K.V. Rao, Micropor. Mater. 2 (1994) 83.
[21] L.S. de Saldarriaga, C. Saldarriaga, M.E. Davis, J. Am. Chem. Soc. 109 (1987) 2686.
[22] A.C. Gujar, A.A. Moye, P.A. Coghill, D.C. Teeters, K.P. Robers, G.L. Price, Micropor. Mesopor. Mater. 78 (2005) 131.
[23] K.H. Schnabel, G. Fingert, T. Kornatowski, E. Löffler, C. Peuker, W. Pilz, Micropor. Mater. 11 (1997) 293.
[24] M. Rokita, M. Handke, W. Mozgawa, J. Mol. Struct. 555 (2000) 351.
[25] S.B. Hong, Micropor. Mater. 4 (1995) 309.
[26] L. Marchese, A. Frache, E. Gianotti, G. Martra, M. Causa‘, S. Coluccia, Micropor. Mesopor. Mater. 30 (1999) 145.
[27] N. Li, Y. Ma, S. Xiang, N. Guan, Chem. Mater. 18 (2006) 975.
[28] L. Vidal, C. Pray, J. Patarin, Micropor. Mesopor. Mater. 39 (2000) 113.
[29] J. Yu, R. Xu, Chem. Soc. Rev. 35 (2006) 593.
[30] B. Han, C. Shin, P.A. Cox, S.B. Hong, J. Phys. Chem. B 110 (2006) 8188.
[31] S.T. Wilson, Stud. Surf. Sci. Catal. 137 (2001) 229.
[32] P. Meriaudeau, V.A. Tuan, V.T. Nghiem, S.Y. Lai, L.N. Hung, C. Naccache, J. Catal. 169 (1997) 55.
[33] D.W. Lewis, C. Richard, A. Catlow, J.M. Thomas, Chem. Mater. 8 (1996) 1112.
[34] M.G. Uytterhoeven, R.A. Schoonheydt, Micropor. Mater. 3 (1994) 265.
[35] F. Rey, G. Sankar, J.M. Thomas, P.A. Barrett, D.W. Lewis, C.R.A. Catlow, S.M. Clark, G.N. Greaves, Chem. Mater. 7 (1995) 1435.
[36] J.A. Martens, M. Mertens, P.J. Grobet, P.A. Jacobs, Stud. Surf. Sci. Catal. 37 (1988) 97.
[37] E.M. Flanigen, R.I. Patton, S.T. Patton, Wilson, in: P.J. Mortier, E.F. Vansant, G. Schulz-Ekloff (Eds.), Innovation in Zeolite Materials Science, Elsevier, Amsterdam, 1988, p. 13.
[38] Ch. Baerlocher, W.H. Meier, D.H. Olson, Atlas of Zeolite Structure Types, Elsevier, Boston, MA, 2001.
[39] B. Lu, T. Tsuda, H. Sasaki, Y. Oumi, K. Itabashi, T. Teranishi, T. Sano, Chem. Mater. 16 (2004) 286.
[40] S. Seelan, A.K. Sinha, J. Mol. Catal. A 215 (2004) 149.
[41] Y. Ma, N. Li, S. Xiang, N. Guan, J. Phys. Chem. C 111 (2007) 18361.
[42] N. Li, Y. Ma, W. Kong, N. Guan, S. Xiang, Micropor. Mesopor. Mater. 115 (2008) 356.
[43] S. Ashtekar, P.J. Barrie, H. Mark, L.F. Gladden, Angew. Chem. Int. Ed. 36 (1997) 876.
[44] N. Khandan, M. Kazemeini, M. Aghaziarati, Appl. Catal. A 349 (2008) 6.
[45] J.M. Campelo, F. Lafont, J.M. Marinas, M. Ojeda, Appl. Catal. A 192 (2000) 85.
[46] J.L.G. Cimadevilla, R. Alvarez, J.J. Pis, Vib. Spectrosc. 31 (2003) 133.
[47] L. Travalloni, A.C.L. Gomes, A.B. Gaspar, A.P.M. da Silva, Catal. Today 133–135 (2008) 406.